




Cite this: *Sens. Diagn.*, 2023, 2, 176

# Detecting low-brominated diphenyl ethers by highly sensitive biosensors based on the blocking effect on glucose oxidase

Xuerui Jiang,<sup>ab</sup> Xiaoyun Bai,<sup>b</sup> Xiaohui Liu,<sup>a</sup>  
 Xuemei Wang <sup>\*a</sup> and Kwok-Keung Shiu<sup>\*b</sup>

Low-brominated diphenyl ether, whose species have an average of 1–4 bromine atoms per molecule, have attracted more and more attention for their high risk of dioxin formation in combustion and effective bioaccumulation in humans and wildlife. Therefore, it is crucial to monitor the level of low-brominated diphenyl ethers. In this study, we fabricated a novel GOD~AuNPs#rGO-CHIT/GC electrode to realize the direct electron transfer of glucose oxidase (GOD) for the determination of BDE-15 based on the blocking effect. The results indicated that the as-prepared GOD~AuNPs#rGO-CHIT/GC electrode can be used for the sensitive detection of two low-brominated diphenyl ethers through the blocking effect on GOD. The linear range for the detection of BDE-15 was 0.2–8  $\mu\text{M}$ , with a sensitivity of 2.86  $\mu\text{A } \mu\text{M}^{-1} \text{ cm}^{-2}$ , and the relevant limits of detection of the two target analytes were 0.14  $\mu\text{M}$  ( $S/N = 3$ ), respectively. This rapid, highly sensitive and cost-effective detection method was also applied to the detection of BDE-3, BDE-28, and BDE-47, which could potentially be used to monitor the levels of PBDEs in our living environment.

Received 8th September 2022,  
 Accepted 13th November 2022

DOI: 10.1039/d2sd00161f

[rsc.li/sensors](https://rsc.li/sensors)

## Introduction

Polybrominated diphenyl ethers (PBDEs) as brominated flame retardants have been widely used in paints, plastic materials, textile fabrics, and electronic equipment to improve the fire resistance of the product for they can release free radicals at high temperatures and block the combustion reaction.<sup>1</sup> On the other hand, the wide application of PBDEs in various fields makes them ubiquitous in air, water, people, soil, birds, fish, and marine mammals.<sup>2,3</sup> In many cases, the concentration of PBDEs is increasing due to the lack of chemical or biological degradation, their high environmental mobility, and their strong tendency for bioaccumulation in the food chain.<sup>4–6</sup> In recent years, more and more attention has been paid to the rising level of PBDEs in the bodies of humans and wildlife, which poses a great risk to human health and the ecological system due to their characteristics of toxicity, mobility, bioaccumulation, and persistence.<sup>7–9</sup> As of April 2022, the United Nations Environment Programme (UNEP) has formally listed tetrabromodiphenyl ether, pentabromodiphenyl ether, hexabromodiphenyl ether, heptabromodiphenyl ether and decabromodiphenyl ether in

Annex A of the Stockholm Convention text as persistent organic pollutants (POPs).

A significant physiological characteristic of PBDEs is that the lower the degree of bromination, the higher the risk of dioxin formation in combustion and more effective bioaccumulation in human and wildlife.<sup>10</sup> Low-brominated diphenyl ethers, whose species average 1–4 bromine atoms per molecule, have been known to affect hormone levels in the thyroid gland, which means that they have higher toxicity to the human nervous system and metabolic system.<sup>11</sup> 4-Bromodiphenyl ether (BDE-3) and 4,4'-dibrominated diphenyl ether (BDE-15) are regarded as ideal research objects for low-brominated diphenyl ethers, for they are the final product of many degradation reactions.<sup>12–15</sup> Consequently, the detection of low-brominated diphenyl ethers is becoming significant in environmental analysis and for human health.

Generally, traditional detection methods for PBDE, including gas chromatography with electron capture detection (GC-ECD),<sup>16</sup> gas chromatography coupled with mass spectrometry (GC-MS),<sup>17</sup> high-performance liquid chromatography combined with mass spectrometry (HPLC-MS),<sup>18</sup> and nuclear magnetic resonance (NMR) spectroscopy,<sup>19,20</sup> are mainly applied in environmental detection, bioaccumulation detection and residual detection in consumer product samples. However, these methods which involve complicated separation and purification steps and potential thermal degradation (bromination of PBDEs)

<sup>a</sup> State Key Lab of Bioelectronics (Chien-Shiung Wu Laboratory), Southeast University, No. 2 Sipailou, Nanjing, China. E-mail: xuemei@seu.edu.cn

<sup>b</sup> Department of Chemistry, Hong Kong Baptist University, Kowloon Tong, Hong Kong SAR, China. E-mail: kkshiu@hkbu.edu.hk



may present a disadvantage. Meanwhile, the advantages of these traditional detection methods are also obvious. Their low detection limit and high detection sensitivity make them widely applicable at trace levels.

In recent years, some new methods without sample separation have been applied to the detection of PBDEs. Raman spectroscopy<sup>21</sup> and fluorescence spectroscopy<sup>22</sup> were innovatively applied in the detection of PBDEs with higher efficiency and lower labour intensity than GC-based methods. Enzyme linked immunosorbent assay (ELISA), one of the most popular enzymatic immunoanalysis methods, has been successfully applied to PBDE analysis.<sup>23,24</sup> However, the disadvantages of ELISA based detection methods are also obvious, such as insufficiency of sensitivity, durability, and portability, and insufficiently fast response.

Electrochemical detection, especially electrocatalytic detection,<sup>25,26</sup> has solved the shortcomings of the above detection technologies and provided a fast, highly sensitive, selective, convenient and cost-effective detection method. An electrochemical sensor is a suitable candidate material for meeting the requirements of cost, size, sensitivity and efficient analysis.<sup>27,28</sup>

Most organic contaminants have inhibition effects on biomacromolecules such as enzymes and nucleic acids. Some enzymatic electrochemical biosensors were made based on the inhibition effect of the target analyte.<sup>29</sup> The concentration of the target analyte can be quantitatively detected according to the electrochemical signal diminution of the substrate catalyzed.<sup>30</sup>

Acetyl cholinesterase (AChE)<sup>31</sup> and colin oxidase<sup>32</sup> have been used for the detection of organophosphorus and

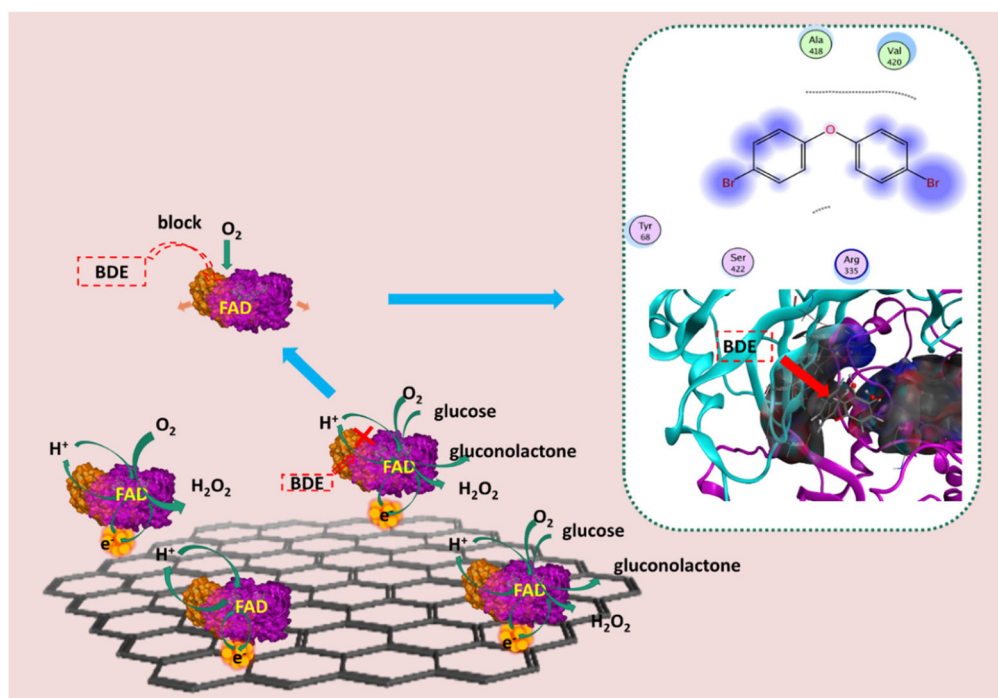
carbamate pesticides. Horseradish peroxidase (HRP)<sup>33</sup> has also been used for the detection of PBDE, PCB, and PBB. However, the application of glucose oxidase (GOD), as an enzymatic electrochemical biosensor, in contamination detection has been rarely reported.

Glucose oxidase, an ideal enzyme, has been widely used to fabricate electrochemical biosensors to detect glucose and H<sub>2</sub>O<sub>2</sub> owing to its low cost, high specific activity, and good stability.<sup>34–36</sup> In this work, GOD was chosen as a sensing element to fabricate an electrochemical biosensor. Reduced graphene oxide (rGO) and gold nanoparticles (AuNPs) were utilized to modify electrodes and improve the properties of the biosensor. Chitosan (CHIT) was chosen as a membrane-forming polymer to immobilize rGO, AuNPs, and GOD. Direct electron transfer of GOD can be achieved at the AuNPs#rGO modified electrode with the immobilization of chitosan (CHIT). The resulting GOD~AuNPs#rGO-CHIT/GC electrode was applied as a glucose biosensor with great sensitivity, and it was further applied for the detection of low-brominated diphenyl ethers including BDE-15 and BDE-3. The principles of determination of low-brominated diphenyl ethers at the GOD~AuNPs#rGO-CHIT/GC electrode are illustrated in Scheme 1.

## Experimental section

### Reagents

Reduced graphene oxide (rGO) was purchased from XFNANO Materials Co. Ltd. (Nanjing, China). Gold(III) chloride trihydrate (HAuCl<sub>4</sub>·3H<sub>2</sub>O), glucose oxidase (GOD) (Type X-)



**Scheme 1** Diagram of the principles of determination of low-brominated diphenyl ether concentration at the GOD~AuNPs#rGO-CHIT/GC based biosensor.



from *Aspergillus niger* (Shanghai, China), D-(+)-glucose, chitosan (CHIT), disodium hydrogen phosphate ( $\text{Na}_2\text{HPO}_4$ ) and sodium phosphate monobasic ( $\text{NaH}_2\text{PO}_4$ ) were obtained from Sigma (Shanghai, China). BDE-3 and BDE-15 were obtained from AccuStandard Inc. (Hong Kong, China). Potassium hexacyanoferrate(III) ( $\text{K}_3\text{Fe}(\text{CN})_6$ ) and potassium ferrocyanide ( $\text{K}_4\text{Fe}(\text{CN})_6$ ) were purchased from International Laboratory (Hong Kong, China). All solutions were prepared with deionized water.

### Apparatus

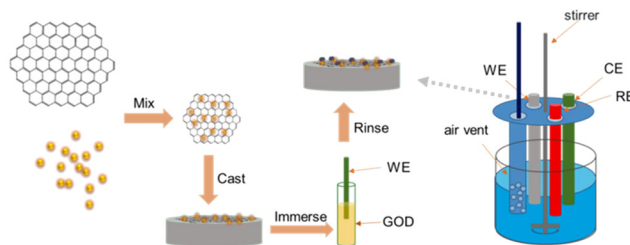
All electrochemical experiments were carried out using a CHI6012B electrochemical analyzer (CH Instruments, Inc., USA). Surface characterization of the modified electrodes was performed with a scanning electron microscope (SEM) (LEO, Electron Microscopy Inc., Cambridge, UK), a transmission electron microscope (TEM) (FEI, FEI Tecnai G2 20 S-TWIN). Electrochemical impedance spectroscopy (EIS) was carried out using a PARSTAT 4000 (AMETEK group of companies).

### Preparation of gold nanoparticles (AuNPs)

AuNPs were prepared by following processes according to Bastus.<sup>37</sup> Typically, 100 mL of deionized water was heated to 100 °C in a three-necked round-bottomed flask with a heating mantle, and 2.2 mL sodium citrate solution (100 mM) was added to boiling water with vigorous stirring. 1 mL  $\text{HAuCl}_4$  (17 mM) was further injected into the above solution, with constant stirring and heating. 15 min later, the solution color changed from pale yellow to soft pink which could be observed due to the generation of AuNPs. The AuNPs were coated with negatively charged citrate ions and, hence, were well-suspended in deionized water.

### Preparation of the modified electrodes

A total of 1 mg rGO was added to 1 mL deionized water to form a homogeneous dark suspension with ultrasonication (denoted as rGO). 1 mg rGO was added to 1 mL of AuNP aqueous solution to form a homogeneous dark suspension with ultrasonication (denoted as AuNPs#rGO). 25 mg chitosan, owing to its high dispersing performance for the graphene material, was dissolved in 10 mL 5% acetic acid solution ( $2.5 \text{ mg mL}^{-1}$ ) as a membrane-forming polymer to immobilize rGO and AuNPs#rGO. 1 mL rGO and 1 mL AuNPs#rGO were respectively added into a 1 mL chitosan solution with ultrasonication to form two homogeneous and stable dark suspensions (denoted as rGO-CHIT and AuNPs#rGO-CHIT). A glassy carbon electrode (GCE, Bioanalytical Systems, Inc., 3 mm in diameter) was carefully polished with 0.3 and 0.05  $\mu\text{m}$  alumina slurry on a MicroCloth (Buehler, USA) and then thoroughly rinsed in ethanol and deionized water by ultrasonication. The clean GC electrode was further activated with 0.1 M  $\text{H}_2\text{SO}_4$  before surface modification (denoted as the bare GC electrode). The AuNPs#rGO-CHIT modified electrode was fabricated by casting a 5  $\mu\text{L}$  AuNPs#rGO-CHIT suspension on the surface



**Scheme 2** Schematic illustration of the procedures used for the construction of the GOD~AuNPs#rGO-CHIT/GC based biosensor.

of the pretreated GC electrode. The modified electrode was allowed to dry in air at ambient temperature. After that, the modified electrode was put in a 60 °C oven for further drying. Graphene can form a thin and uniform film on the GCE surface through  $\pi$ - $\pi$  electronic interactions between graphene and GC (denoted as the AuNPs#rGO-CHIT/GC electrode). The same procedures were employed to assemble the rGO-CHIT/GC electrode. Afterwards, the AuNPs#rGO-CHIT/GC electrode was immersed into the GOD solution ( $5 \text{ mg mL}^{-1}$ , pH 6.0, PBS) for 10 h at 4 °C to assemble the GOD~AuNPs#rGO-CHIT/GC electrode. The modified electrode was further rinsed with deionized water and stored at a 4 °C nitrogen environment until use (denoted as the GOD~AuNPs#rGO-CHIT/GC electrode). The same procedures were employed to assemble the GOD~/rGO-CHIT/GC electrode. The procedures used for the construction of the relevant biosensor are shown in Scheme 2.

### Electrochemical characterization of the modified electrode

Phosphate buffer solution (PB solution) consisting of 0.1 M  $\text{PO}_4^{3-}$  and 0.1 M KCl was used as the supporting electrolyte. Potassium ferricyanide solution (5 mM) consisting of 5 mM  $\text{K}_3\text{Fe}(\text{CN})_6$ , 5 mM  $\text{K}_4\text{Fe}(\text{CN})_6$  and 0.1 M KCl was used as the impedance electrolyte for electrochemical impedance spectroscopy (EIS). Cyclic voltammetry was carried out to assess the assembly performance of the modified electrode in PB solution (pH 7.3), with potential values ranging from -1 V to 1 V at  $100 \text{ mV s}^{-1}$ . Electrochemical impedance spectroscopy (EIS) was carried out in 5.0 mM  $\text{K}_3\text{Fe}(\text{CN})_6$  containing 0.1 M KCl in a frequency range from 0.1 to 10 kHz under open-circuit potential conditions. Experimental conditions consisting of different scan rates, pH values, and ventilations were compared by cyclic voltammetry to characterize the influence of experimental conditions at the modified electrode in PB solution (pH 6.0) with potential values ranging from -0.8 to 0 V at  $50 \text{ mV s}^{-1}$ . The current response was recorded on successive addition of the substrates.

### Procedure for the determination of glucose, BDE-3 and BDE-15

D-(+)-glucose was dissolved in PB solution (pH 6.0); BDE-3 and BDE-15 were dissolved in ether and they were further





dispersed in PB solution to obtain stable solutions as target analytes. Cyclic voltammetry was carried out in an air-saturated PB solution to characterize the change of redox current at the modified electrode in the presence of target analytes, with potentials ranging from  $-0.8$  to  $0$  V at  $50$  mV  $s^{-1}$ . The steady-state amperometric responses to glucose and BDEs were measured in an air-saturated PB solution (pH 6.0) under gentle stirring at around  $30$  rpm at the desired potentials, respectively. The current response was recorded on successive addition of the target analytes. After each experiment the enzyme electrode activity was regenerated by rinsing the electrode with double distilled water. BDE-3 was prepared and detected through the same procedure as BDE-15.

## Results and discussion

### Characterization of materials for electrode modification

TEM was first used for the characterization of rGO and the AuNPs#rGO suspension, which was dispersed by chitosan-acetic acid. The nanosheet structure of rGO (Fig. 1A) showed good ductility and a single layer, which meant high electrical conductivity and good film-forming properties. The AuNPs were reduced by citrate sodium anchored on the surface of rGO with relatively uniform particles (Fig. 1B). SEM was used to characterize the surface of the rGO-CHIT/GC electrode and the GOD~/AuNPs#rGO-CHIT/GC electrode. As can be seen in Fig. 1C, with the addition of AuNPs and the fabrication of GOD, apparent particles appeared on the surface of the

chitosan. The particle diameter distribution (Fig. 1D) was obtained with Nano Measurer software. The particle diameter distribution of AuNPs on rGO follows a normal distribution, with a mean size of about  $10$  nm. The results proved that small AuNPs particles can be obtained through the reduction of citrate sodium. The particle diameter of the GOD~/AuNPs composites also showed a normal distribution. However, the mean particle size of the GOD~/AuNPs composites increased from  $10$  nm to  $17$  nm against AuNPs, with a wider distribution. Given that the molecular size of GOD was also a few nanometers, these results indicated that GOD was successfully combined with AuNPs.

As an enzyme linker, AuNPs were mainly applied owing to its high adhesion to GOD and rGO. rGO played an important role in this electrochemical detection; on the one hand, it enhanced the embedding of AuNPs and GOD, on the other hand, its oxidation sites were used to increase the coupling characteristics with the electrode substrate. Besides, in order to enhance the stability of the electrode, a chitosan film was formed on the new electrode.

### Electrochemical characterization of the modified electrodes

Cyclic voltammograms (CVs) of the GOD~/AuNPs#rGO-CHIT (black line), AuNPs#rGO-CHIT (red line), GOD~/AuNPs-CHIT (blue line) and GOD~/rGO-CHIT (green line) modified electrodes in PB solution (pH 7.3) are shown in Fig. 2A. Compared with the AuNPs#rGO-CHIT/GC electrode, the CV of the GOD~/AuNPs#rGO-CHIT/GC electrode showed two

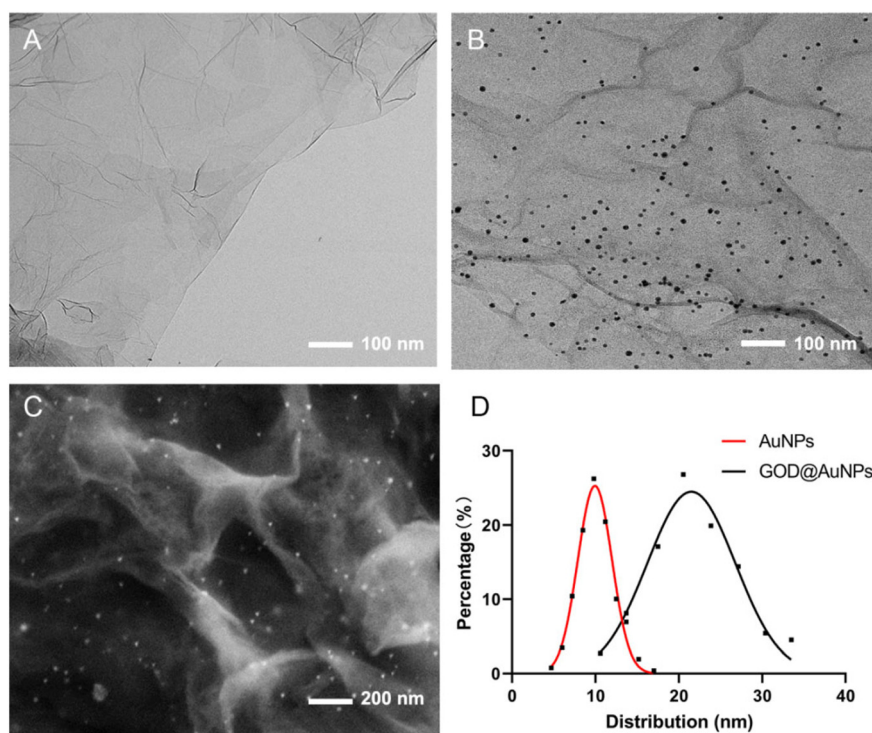
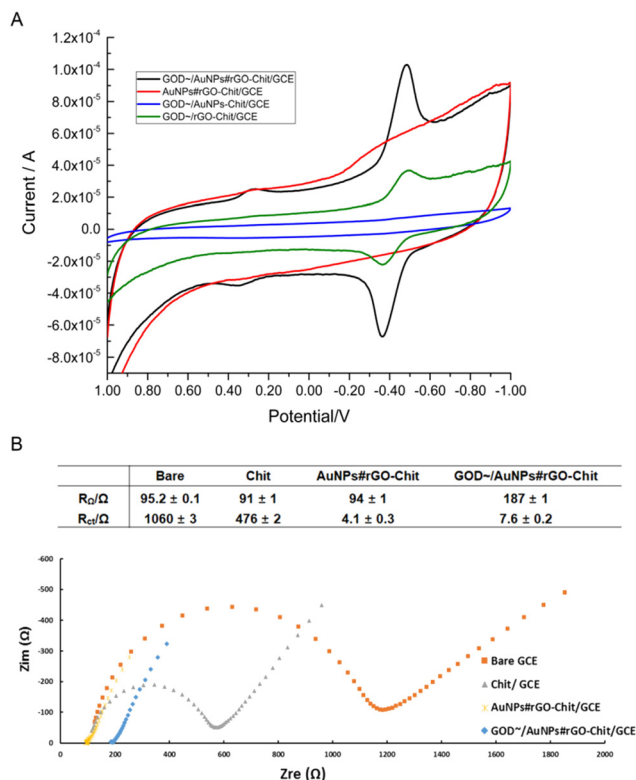


Fig. 1 TEM characterization of rGO (A) and AuNPs#rGO (B) SEM characterization of the GOD~/AuNPs#rGO-CHIT/GC electrode (C) and particle diameter distribution of AuNPs and GOD@AuNPs (D).





**Fig. 2** Cyclic voltammograms of GOD~AuNPs#rGO-CHIT (black line), AuNPs#rGO-CHIT (red line), GOD~AuNPs-CHIT (blue line) and the GOD~rGO-CHIT modified electrode in 0.1 M PB solution (pH 7.3); scan rate:  $0.1 \text{ V s}^{-1}$  (A). Nyquist plots of the electrochemical impedance spectroscopy (EIS) measurements in 5 mM  $[\text{Fe}_{3/4}(\text{CN})_6]^{3-/4-}$  solution containing 0.1 M KCl at the bare GC electrode (orange solid squares), CHIT (gray solid triangles), AuNPs#rGO-CHIT (yellow solid forks) and the GOD~AuNPs#rGO-CHIT (blue solid diamonds)-modified GC electrode (B).

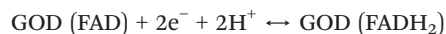
groups of redox peaks. One of them appeared at 0.265 V and 0.356 V, while the other redox peaks occurred at other potentials (−0.484 V and −0.364 V), the latter two were the characteristic redox peak potentials of FAD. This indicated that GOD was successfully combined with the surface of the AuNPs#rGO-chitosan membrane, and direct electron transfer was realized between GOD and the membrane. The redox peak current of the GOD~rGO-CHIT/GC electrode, as well as the baseline, was lower than that of the GOD~AuNPs#rGO-CHIT/GC electrode. This indicated that the existence of AuNPs remarkably enhanced the electron transfer efficiency between the modified electrode and electrolyte. As for the CV of the GOD~AuNPs-CHIT/GC electrode, compared with the others, the lowest baseline and the disappearance of redox peaks indicated that rGO played a role of connecting the GCE surface and other modified components.

Electrochemical impedance spectroscopy (EIS) is an effective method to characterize the heterogeneous electron transfer efficiency of the modified electrode surface.<sup>38,39</sup> We can obtain the values of the ohmic resistance ( $R_{\Omega}$ ) and the charge transfer resistance ( $R_{ct}$ ) from the Nyquist plots by EIS. Nyquist plots of chitosan (gray solid triangles), AuNPs#rGO-chitosan (yellow

solid forks) and GOD~AuNPs#rGO-chitosan (blue solid diamonds)-modified and bare GCE (orange solid square) in 5 mM  $[\text{Fe}_{3/4}(\text{CN})_6]^{3-/4-}$  containing 0.1 M KCl are displayed in Fig. 2B.

The values of  $R_{\Omega}$  and  $R_{ct}$  were calculated with the software ZView 3.0 according to the information obtained from the Nyquist plots. The results showed that the bare GC electrode, CHIT/GC electrode and AuNPs#rGO-CHIT/GC electrode had similar  $R_{\Omega}$  (90–95  $\Omega$ ) values, while the  $R_{\Omega}$  value of the GOD~AuNPs#rGO-CHIT/GC electrode ( $187 \pm 1 \text{ } \Omega$ ) was two times as high as those of the other electrodes. This could be attributed to the fact that GOD was not deeply embedded in the chitosan membrane but attached to the membrane surface by the non-electrostatic force of −SH and AuNPs, which could block electron transfer between the electrochemical probe and the electrode surface as a series resistor. The value of the transfer resistance ( $R_{ct}$ ) gradually decreased with the addition of the modifiers. The  $R_{ct}$  value of the CHIT/GC electrode ( $476 \pm 2 \text{ } \Omega$ ) was half the value of the bare GC electrode ( $1060 \pm 1 \text{ } \Omega$ ); the addition of AuNPs#rGO would further greatly reduce the  $R_{ct}$  value of the AuNPs#rGO-CHIT/GC electrode ( $4.1 \pm 0.3 \text{ } \Omega$ ). By comparison, the  $R_{ct}$  value of the GOD~AuNPs#rGO-CHIT/GC electrode ( $7.6 \pm 0.2 \text{ } \Omega$ ) was slightly higher than that of the AuNPs#rGO-CHIT/GC electrode. The results indicated that the chitosan membrane can be firmly fabricated on the surface of the GC electrode, combining with fresh carbon points and increasing the specific surface area of the electrode. In addition, rGO played the role of an electron transfer linker owing to its high electron transfer efficiency of the  $\pi$ - $\pi$  electron layer.<sup>38,40</sup>

The effect of pH on the potential could be shown by the CVs of the GOD~AuNPs#rGO-chitosan modified GC electrode in PB solution with pH values ranging from pH 5.5 to pH 7.0 (Fig. 3A). With the increase in pH value, the anodic and cathodic peak potentials of the modified electrode decreased linearly, as shown in Fig. 3B. The linear regression equations for the potentials and pH were  $E_{pa}(\text{V}) = -0.024 - 0.058 \times \text{pH}$ ,  $R^2 = 1$  and  $E_{pc}(\text{V}) = -0.0805 - 0.0556 \times \text{pH}$ ,  $R^2 = 0.9995$ . The linear slope of  $E_{pa} - \text{pH}$  equaled to  $58 \text{ mV pH}^{-1}$  and that of  $E_{pc} - \text{pH}$  equaled to  $55.6 \text{ mV pH}^{-1}$ . Both of them are very close to the theoretical Nernst's limit ( $59 \text{ mV pH}^{-1}$ ,  $20^\circ\text{C}$ )<sup>41</sup> as reported, indicating that a proton-electron reaction occurred on the surface of the modified electrodes, where the number of electrons transferred is equal to the number of protons. This indicated that GOD (FAD) participated in the following reversible reaction as seen in the equation:



Typical CVs of the GOD~AuNPs#rGO-chitosan modified GC electrode in 0.1 M PB solution (pH 6.0) at a series of scan rates ranging from 10 to 500  $\text{mV s}^{-1}$  (Fig. 3C) showed the effect of the scan rate. With an increase in scan rate, the anodic and cathodic peak potentials of the modified electrode showed a small shift while the redox peak currents increased linearly (shown in Fig. 3D). The linear regression equations were  $I_{pa}(\mu\text{A}) = -2.2745 - 0.1647 \times \text{SC}(\text{mV s}^{-1})$ ,  $R^2 = 0.9975$  and  $I_{pc}(\mu\text{A}) = 4.084$



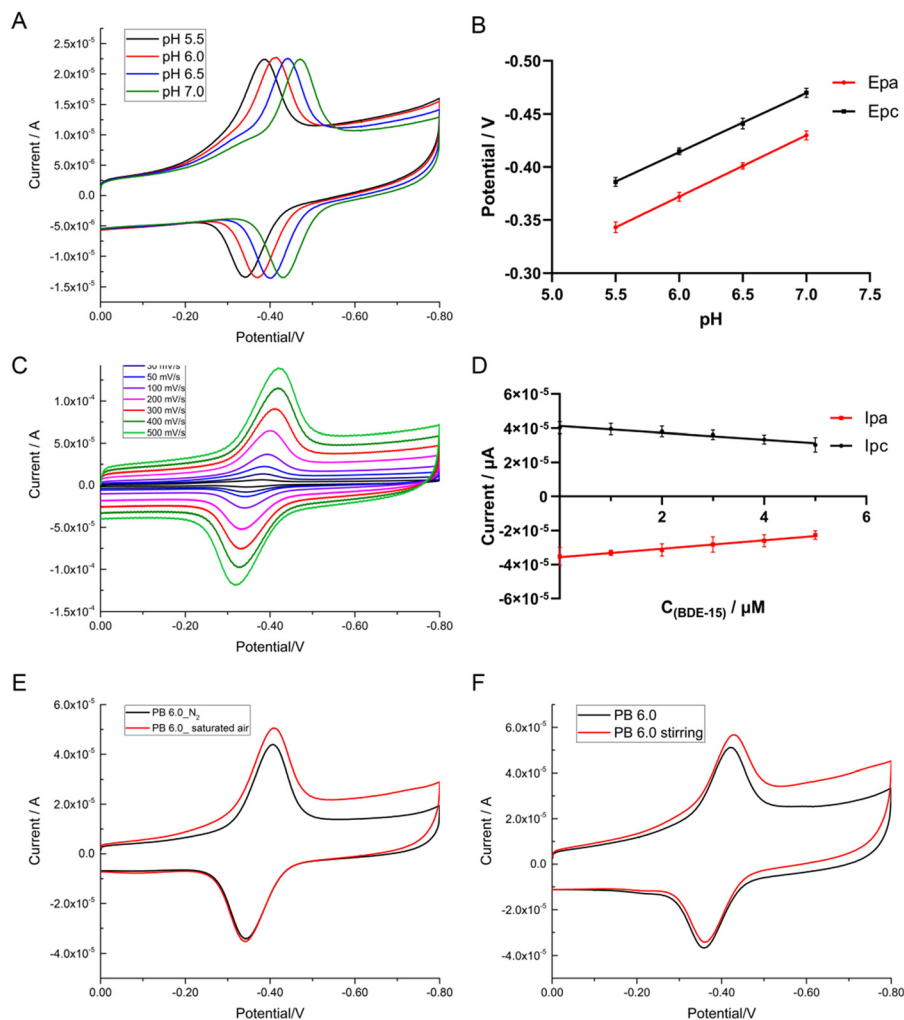
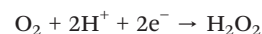
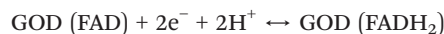


**Fig. 3** Cyclic voltammograms of the GOD~AuNPs/rGO-CHIT/GC electrode in 0.1 M PB solution (pH 6.0, 0.1 M KCl) at pH 5.5, 6.0, 6.5, and 7.0; scan rate: 50 mV s<sup>-1</sup> (A). Scatter plots of the cathodic and anodic peak potentials versus pH (B) at a series of scan rates from 10 to 500 mV s<sup>-1</sup> (from inner to outer) (C). Scatter plots of the cathodic and anodic peak currents versus the scan rates (D). Cyclic voltammograms of the GOD~AuNPs/rGO-CHIT/GC electrode in 0.1 M PB solution (pH 6.0, black line) in saturated air (pH 6.0, red line) (E) and in air-saturated PB solution (pH 6.0, black line) with gentle stirring (pH 6.0, red line) (F); scan rate: 50 mV s<sup>-1</sup>.

+ 0.188 × SC (mV s<sup>-1</sup>),  $R^2 = 0.996$ , indicating that the electron transfer reaction of the modified electrode was a surface-controlled quasi-reversible behavior.<sup>42</sup> According to the Laviron equation:  $I_p = nFQv/4RT$ , the average electron transfer number was calculated to be 1.6. In this equation,  $F$  stands for Faraday's constant (96 485.3365 C mol<sup>-1</sup>),  $R$  stands for the gas constant (8.314472 J K<sup>-1</sup> mol<sup>-1</sup>),  $T$  stands for the thermodynamic temperature (298 K), and  $Q$  stands for the electrical quantity, provided by the instrument, of one reaction process.

We changed the experimental conditions for cyclic voltammetry by air-blowing and stirring. We blew air into the PB solution (pH 6.0) for 10 min to obtain an air-saturated solution before electrochemical detection. CVs of the modified electrode in air-saturated PB solution are shown in Fig. 3E, indicating that the current of the cathodic peak rose obviously, while the potential had a slight right shift. At the same time, the current and potential of the anodic peak remained unchanged. Similar results were achieved in the process of

stirring, as shown in Fig. 3F, indicating that the cathodic and anodic peak currents rose obviously, while the peak potential had a slight right shift. This indicated that the reversible redox current, which was caused by GOD (FAD/FADH<sub>2</sub>), was very stable, and the rise of the cathodic peak current was caused by the reduction of dissolved oxygen with the participation of H<sup>+</sup> and e<sup>-</sup>, as seen in the following equations:



#### Direct electrochemistry detection of glucose and BDE-15

As is known, GOD has a high catalytic activity toward glucose oxidation. In our work, direct electrochemistry detection of



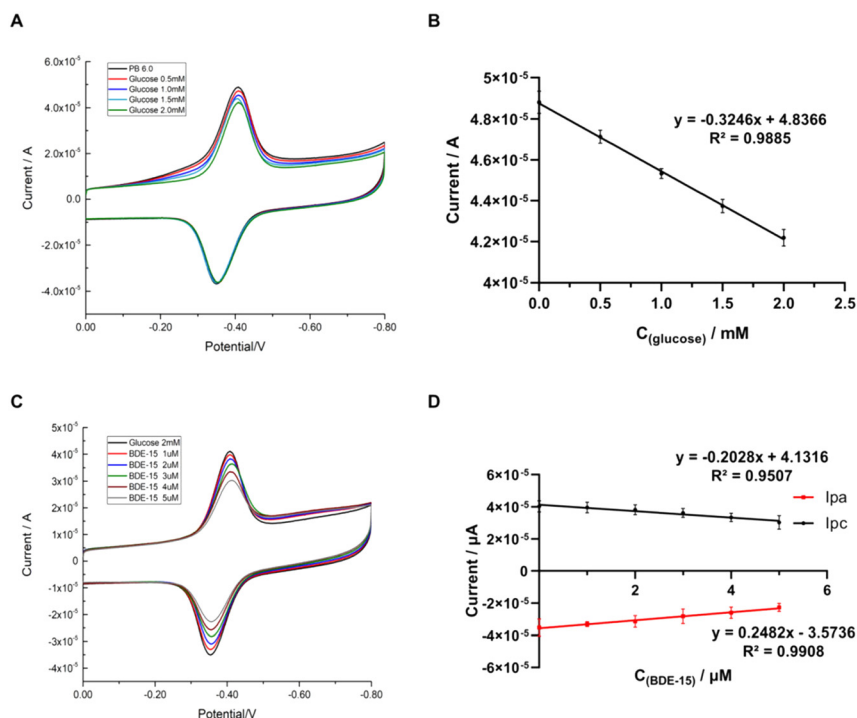
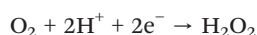


**Fig. 4** Cyclic voltammograms of the GOD~AuNPs#rGO-CHIT/GC electrode in 0.1 M PB solution (pH 6.0, 0.1 M KCl), with the concentration of glucose ranging from 0 to 2 mM; scan rate:  $50 \text{ mV s}^{-1}$  (A). Scatter plot of the cathodic peak current versus the glucose concentration (B). Cyclic voltammograms of the GOD~AuNPs#rGO-CHIT/GC electrode in 0.1 M PB solution (pH 6.0, 0.1 M KCl, 2 mM glucose), with the concentration of BDE-15 ranging from 0 to 5  $\mu\text{M}$ ; scan rate:  $50 \text{ mV s}^{-1}$  (C). Scatter plots of the cathodic and anodic peak currents versus the BDE-15 concentration (D).

glucose was used to evaluate the catalytic performance of the GOD~AuNPs#rGO-CHIT/GC electrode by cyclic voltammetry in 0.1 M air-saturated PB solution (pH 6.0). The cyclic voltammograms (CVs), presented in Fig. 4, were obtained in different concentrations of glucose. As shown in Fig. 4A, with the increase in glucose concentration, the anodic peak current remained unchanged, while the cathodic peak current decreased linearly. The current linearly responded to the concentration of glucose (Fig. 4B), with the linear regression equation being  $I_{pc} (10 \mu\text{A}) = 4.8366 - 0.3246 \times C_{\text{glucose}} (\text{mM})$ ,  $R^2 = 0.9885$ . This indicated that glucose participated in reactions as seen in the following equations:



The cathodic peak current decreased, as shown in Fig. 4A, which was caused by the consumption of oxygen during the oxidation of glucose, under the catalysis of GOD.

The detection of BDE-15 was further carried out based on glucose detection. As shown in the CVs (Fig. 4C) of the modified electrodes in air-saturated PB solution (pH 6.0) containing 2 mM glucose, the anodic and cathodic peak

currents decreased simultaneously and linearly, with an increase in the concentration of BDE-15 from 0 to 5  $\mu\text{M}$ . The scatter plots of the anodic and cathodic peak currents versus the concentration of BDE-15 showed a linear relationship between  $C_{\text{BDE-15}}$  and current (Fig. 4D). The linear regression equations were  $I_{pc} (10 \mu\text{A}) = 4.1316 - 0.2028 \times C_{\text{BDE-15}} (\mu\text{M})$ ,  $R^2 = 0.9507$  and  $I_{pa} (10 \mu\text{A}) = -3.5736 - 0.2482 \times C_{\text{BDE-15}} (\mu\text{M})$ ,  $R^2 = 0.9908$ . The results indicated that the existence of BDE-15 affected the redox reaction of GOD (FAD/FADH<sub>2</sub>). In view of the fact that there was no direct reaction between BDE-15 and FAD/FADH<sub>2</sub>, which could consume the total amount of FAD/FADH<sub>2</sub>, the only explanation for this decrease was that BDE-15 might have blocked the exchange of protons between the electrolyte and FAD/FADH<sub>2</sub>, thus resulting in the reduction of the redox peak current.

#### Amperometric detection of glucose and BDE-15

According to the catalytic activity of glucose and the blocking effect of BDE-15 on GOD activity, the GOD~AuNPs#rGO-CHIT/GC electrode was further used for the determination of target analytes by means of an amperometric  $I-t$  curve. Fig. 5 shows the detection of glucose at the GOD~AuNPs#rGO-CHIT/GC electrode in air-saturated PBS solution (pH 6.0) by gently stirring at an applied potential of  $-0.4 \text{ V}$ . The baseline current decreased continuously upon successive addition of glucose due to the consumption of oxygen. The results indicated that the GOD~AuNPs#rGO-CHIT/GC electrode had good catalytic activity





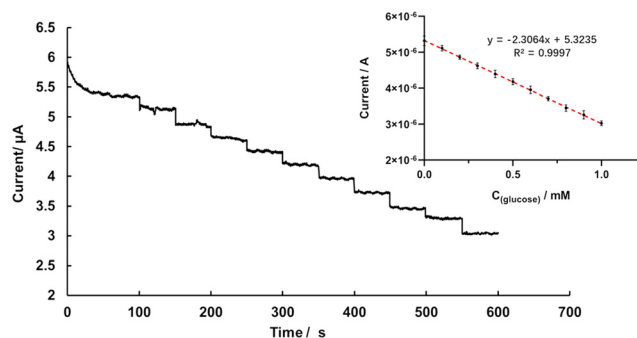


**Fig. 5** Amperometric  $I$ - $t$  curve for the GOD~/AuNPs#rGO-CHIT/GC electrode in 0.1 M PB solution (pH 6.0), with the concentration of glucose ranging from 0.1 to 1 mM at  $-0.4$  V; inset: scatter plot of response current ( $\mu$ A) versus  $C_{(\text{glucose})}/\text{mM}$ .

toward glucose oxidation. The inserted scatter plot in Fig. 6 is the resulting calibration curve for glucose detection at the GOD~/AuNPs#rGO-CHIT/GC electrode. A linear response for the glucose concentration was observed from 0.1 to 1 mM with a detection limit of  $50 \mu\text{M}$  ( $S/N = 3$ ). The sensitivity was calculated to be  $32.4 \mu\text{A mM}^{-1} \text{cm}^{-2}$ .

The detection of BDE-15 and glucose at the GOD~/AuNPs#rGO-CHIT/GC electrode in the stirred air-saturated PBS solution (pH 6.0) at an applied potential of  $-0.4$  V is shown in Fig. 6. After the baseline current became steady, we added  $0.2 \mu\text{M}$  BDE-15 to the PB solution every 50 seconds. In the beginning, the baseline current decreased obviously, but this reduction became less and less obvious after the addition of  $0.6 \mu\text{M}$  BDE-15. When the concentration of BDE-15 approached  $2 \mu\text{M}$ , it was hard to distinguish whether BDE-15 was added or not. After that, we paused the detection

and blew new air into the solution for 30 s, keeping the electrolytic cell on. The detection continued after the solution was stabilized and a significant decrease in current could be observed in the same solution after new air was blown in. This indicated that  $\text{O}_2$  played an important role in the combination of BDE-15 and GOD.

Afterwards,  $2 \mu\text{M}$  BDE-15 was dropped into the solution each time, with new air blown in for 30 s, and the baseline current became steady again at around  $9 \mu\text{M}$ . The scatter plot of the current and  $C_{(\text{BDE-15})}$  showed a linear response between 0.2 and  $8 \mu\text{M}$ , the linear regression equation being  $I (\mu\text{A}) = 5.8226 - 0.2028 \times C_{(\text{BDE-15})} (\mu\text{M})$ ,  $R^2 = 0.9972$ . The sensitivity was calculated to be  $2.86 \mu\text{A } \mu\text{M}^{-1} \text{cm}^{-2}$  with a limit of detection of  $0.14 \mu\text{M}$  ( $S/N = 3$ ). Later on, glucose was added to the above solution to test the catalytic performance of GOD,  $0.25 \text{ mM}$  glucose each time. The calibration curve for glucose detection showed a linear response between 0.25 to 1 mM, the linear regression equation being  $I (\mu\text{A}) = 4.0232 - 2.1536 \times C_{(\text{glucose})} (\text{mM})$ ,  $R^2 = 0.9956$ ; the sensitivity was calculated to be  $30.33 \mu\text{A mM}^{-1} \text{cm}^{-2}$  with a limit of detection of  $46 \mu\text{M}$  ( $S/N = 3$ ). The amperometric detection of BDE-15 and glucose in the air-saturated PB solution (pH 6.0) indicated a linear response of the current versus  $C_{(\text{BDE-15})}$  and  $C_{(\text{glucose})}$ .

Further experiments compared the decreasing trend of current in PBS containing  $5 \mu\text{M}$  BDE-15 (pH 6.0) with gradual addition of glucose, as shown in the amperometric  $I$ - $t$  curve (Fig. 7A) and the Lineweaver-Burk plot (Fig. 7B). When the GOD~/AuNPs#rGO-CHIT/GC electrode was immersed into PBS in the presence of glucose at an applied potential of  $-0.4$  V, glucose was enzymatically oxidized by GOD immobilized on the surface of the electrode to form gluconic acid, and  $\text{O}_2$

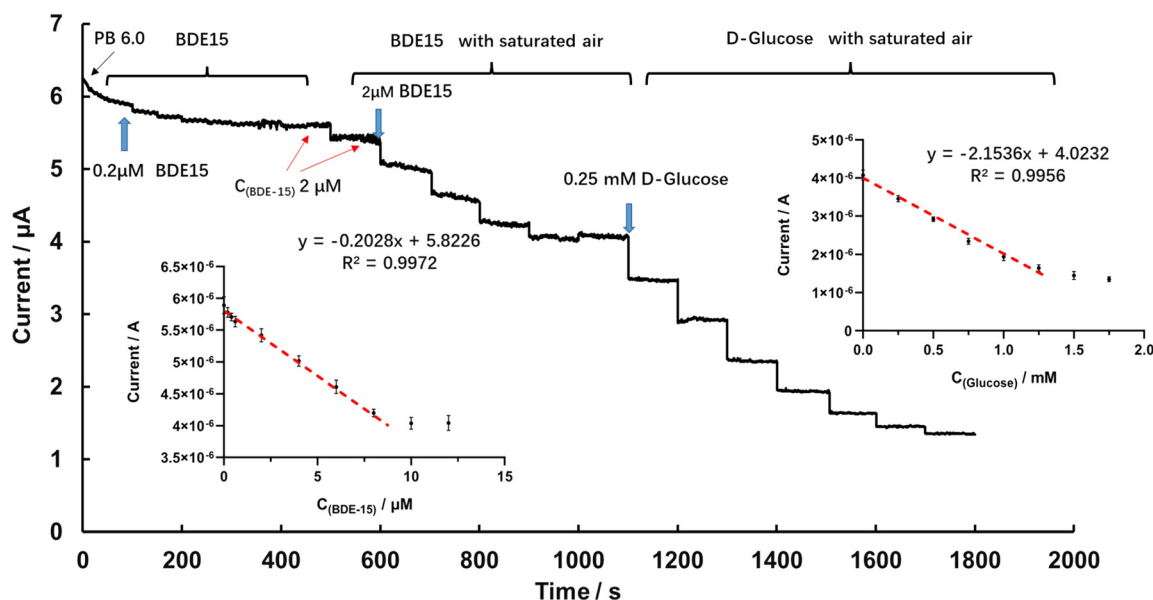


**Fig. 6** Amperometric  $I$ - $t$  curve for the GOD~/AuNPs#rGO-CHIT/GC electrode in 0.1 M PB solution (pH 6.0), with the concentration of BDE-15 ranging from 0.2 to  $12 \mu\text{M}$  and the concentration of glucose ranging from 0.25 to  $1.75 \text{ mM}$  at  $-0.4$  V; insets: scatter plots of the response current ( $\mu$ A) versus  $C_{(\text{glucose})}/\text{mM}$  and  $C_{(\text{BDE-15})}/\mu\text{M}$ .



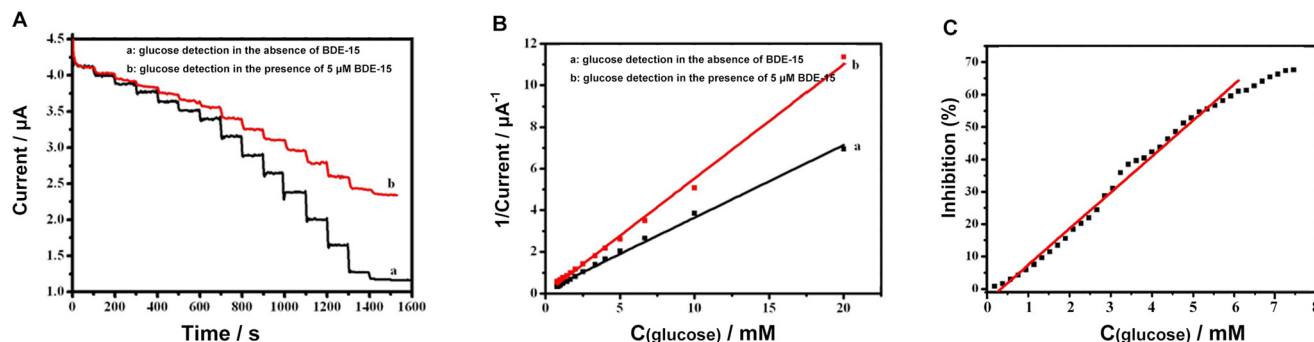


Fig. 7 GOD~AuNPs#rGO-CHIT/GC electrode response to successive addition of glucose in the absence a) and presence b) of 5  $\mu\text{M}$  BDE-15 in air-saturated PBS (pH 6.0) at  $-0.4$  V. (B): Lineweaver-Burk plot for GOD response to glucose in the absence a) and presence b) of 5  $\mu\text{M}$  BDE-15 in air-saturated PBS (pH 6.0) at  $-0.4$  V. (C): Inhibition calibration curve for BDE-15 against GOD.

was reduced to form  $\text{H}_2\text{O}_2$  at the same time. This induced a dramatic decrease of the current due to the consumption of  $\text{O}_2$ . However, the catalytic activity of GOD toward glucose oxidation was inhibited upon the addition of PBDEs, which reduced the oxidation of glucose and the consumption of  $\text{O}_2$ . Therefore, the GOD~AuNPs#rGO-CHIT/GC biosensor can be applied for the determination of PBDEs based on the inhibition effect of PBDEs on GOD.

Usually, the inhibition capability of PBDEs towards GOD activity can be judged using the percent of inhibition ( $I\%$ ), which can be calculated using the following relationship:

$$I\% = 100 \times (I_0 - I_i) / I_0$$

In this relationship,  $I_0$  and  $I_i$  represent the steady-state current of a final concentration of glucose and

the steady-state current after the successive addition of PBDEs in the electrolyte, respectively. The resulting calibration curve for the inhibition capability towards GOD activity against the concentration of BDE-15 (Fig. 7C). The concentration of BDE-15 changed from 0.2 to 8  $\mu\text{M}$ , resulting in variation of the inhibition capability from 0.84% to 67.58%. In addition, the inhibition percentages and 50% inhibition ( $\text{IC}_{50}$ ) are important parameters.

The results indicated that the catalytic activity of glucose was not greatly affected by the existence of BDE-15 but more related to dissolved oxygen. Then, the decrease in current caused by BDE-15 indicated that BDE-15 could attach to GOD and affect the exchange of protons between GOD ( $\text{FAD}/\text{FADH}_2$ ) and the electrolyte, with the assistance of dissolved oxygen.

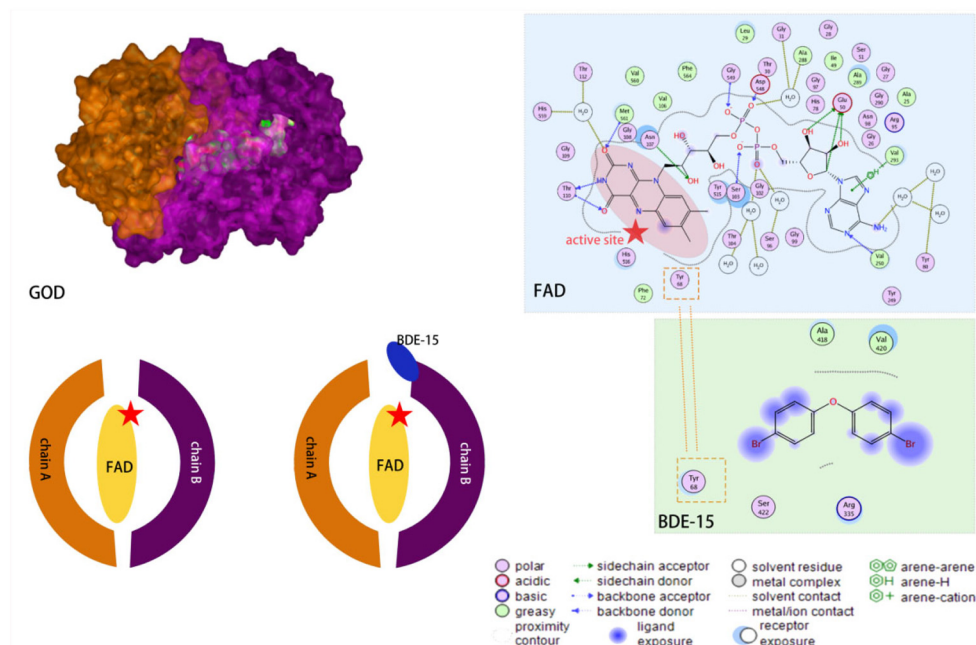


Fig. 8 Protein model and molecular docking model of BDE-15 and GOD.



**Table 1** The results for the detection of all the four BDEs

BDEs	Linear range ( $\mu\text{M}$ )	Sensitivity ( $\mu\text{A } \mu\text{M}^{-1} \text{ cm}^{-2}$ )	LOD ( $\mu\text{M}$ )	$R^2$	S/N
BDE-3	1–6	3.05	0.42	0.99237	3
BDE-15	0.2–8	2.86	0.14	0.99339	3
BDE-28	0.42–5.4	9.9	0.23	0.99663	3
BDE-47	0.9–3.5	8.2	0.54	0.99537	3

### Molecular docking of GOD and BDE-15

To validate the research conclusions above, molecular docking of GOD and BDE-15 was conducted with the assistance of the software MOE to visualize the interaction. GOD's macromolecule structure, whose protein code is 1CF3, was downloaded from the PDB database. Two main domains, like two shells, are shown in Fig. 8. FAD, retained as the active site, was deeply embedded in the GOD. The surface plot of the pocket of FAD looked like a tunnel with its top looking like a rift valley. BDE-15 was imported as a ligand and it could easily adhere to the rift valley between two domains when we minimized energy. The ligand-binding pocket of BDE-15 was near the top of the ligand-binding pocket of FAD. As shown in the ligand interaction plot, the benzene ring tended to be exposed to the nonpolar amino acid residues (Ala, 418; Val, 420), while 4,4'-bromine tended to be exposed to the polar amino acid residues (Tyr, 68; Ser, 422; Arg, 335). In particular, for the amino acid residue (Tyr, 68), it was very close to the active site of FAD in space; at the same time, it was the main exposure site of ligand BDE-15. These results mean BDE-15 had a tendency to get close to the rift valley of GOD. Like an obstacle in front of a gate, BDE-15 might block the exchange of protons between GOD (FAD) and electrolytes.

### Amperometric detection of PBDEs including BDE-3, BDE-28 and BDE-47

According to the inhibition effect of BDE-15 on GOD activity, GOD~AuNPs/rGO-CHIT/GC was further used for the determination of PBDEs, including BDE-3, BDE-28 and BDE-47, by the detection of glucose in a stirred air-saturated PBS solution (pH 6.0) at an applied potential of  $-0.4$  V. The results for the detection of all the BDEs are presented in Table 1. The GOD~AuNPs/rGO-CHIT/GC biosensor displayed a large linear range and a relatively high sensitivity for the four BDEs in aqueous media (pH 6.0 PBS). Furthermore, the selectivity of the biosensor was also investigated for the detection of BDEs in the presence of citrate, chloride, sulfate and carbonate at an applied potential of  $-0.4$  V. The results indicated that the interference from citrate, chloride, sulfate and carbonate was negligible for the detection of the four BDEs.

## Conclusions

A simple and effective electrochemical biosensor based on the blocking effect on GOD was fabricated to detect low-brominated diphenyl ethers, including BDE-3, BDE-15, BDE-

28 and BDE-47. Chitosan was used as a basement membrane to support modifiers. A AuNPs/rGO composite was used for the modification of the electrode to improve the properties of the electrode. GOD could be readily immobilized on the surface of the AuNPs/rGO/GC electrode to construct the GOD~AuNPs/rGO-CHIT/GC electrode through the efficient interaction of  $-\text{SH}$  with AuNPs. Then, the direct electron transfer of GOD was achieved at the AuNPs/rGO-CHIT modified electrode. The as-prepared GOD~AuNPs/rGO-CHIT/GC electrode was utilized for the sensitive determination of glucose. Then, the GOD~AuNPs/rGO-CHIT/GC electrode was further applied successfully for the detection of low-brominated diphenyl ethers, according to the blocking effect of low-brominated diphenyl ethers on GOD with good sensitivity and a wide linear range. This rapid, highly sensitive and cost-effective detection strategy could potentially be applied to monitor the levels of PBDEs in our living environment.

## Author contributions

Data curation: X. J. and X. B.; formal analysis: X. L.; funding acquisition: K. S. and X. W.; investigation: K. S. and X. W.; methodology: X. J.; resources: K. S. and X. W.; software: X. J. and X. B.; supervision: K. S. and X. W.; validation: X. J. and X. B.; visualization: X. J.; writing—original draft: X. J.; writing—review and editing: X. L., K. S. and X. W. All the authors have read and agreed to the published version of the manuscript.

## Conflicts of interest

There are no conflicts to declare.

## Acknowledgements

This work was supported by the Partner State Key Laboratory of Environmental and Biological Analysis of Hong Kong Baptist University (SKLP/14-15/P007), the National Natural Science Foundation of China (Grant No. 82061148012, 82027806), and the National High Technology Research & Development Program of China (2017YFA0205300).

## References

- H. M. Stapleton, S. Klosterhaus, A. Keller, P. L. Ferguson, S. van Bergen, E. Cooper, T. F. Webster and A. Blum, Identification of Flame Retardants in Polyurethane Foam Collected from Baby Products, *Environ. Sci. Technol.*, 2011, **45**, 5323–5331.
- J. L. N. Sprowles, S. Monaikul, A. Aguiar, J. Gardiner, N. Monaikul, P. Kostyniak and S. L. Schantz, Associations of concurrent PCB and PBDE serum concentrations with executive functioning in adolescents, *Neurotoxicol. Teratol.*, 2022, **92**, 107092.
- S. Neumann, M. Harju, D. Herzke, T. Anker-Nilssen, S. Christensen-Dalsgaard, M. Langset and G. W. Gabrielsen, Ingested plastics in northern fulmars (*Fulmarus glacialis*): A



- pathway for polybrominated diphenyl ether (PBDE) exposure?, *Sci. Total Environ.*, 2021, **778**, 146313.
- 4 K. Gustafsson, M. Bjork, S. Burreau and M. Gilek, Bioaccumulation kinetics of brominated flame retardants (polybrominated diphenyl ethers) in blue mussels (*Mytilus edulis*), *Environ. Toxicol. Chem.*, 1999, **18**, 1218–1224.
  - 5 G. T. Tomy, K. Pleskach, T. Oswald, T. Halldorson, P. A. Helm, G. Macinnis and C. H. Marvin, Enantioselective bioaccumulation of hexabromocyclododecane and congener-specific accumulation of brominated diphenyl ethers in an eastern Canadian Arctic marine food web, *Environ. Sci. Technol.*, 2008, **42**, 3634–3639.
  - 6 J. P. Wu, Y. Zhang, X. J. Luo, Y. Z. She, L. H. Yu, S. J. Chen and B. X. Mai, A review of polybrominated diphenyl ethers and alternative brominated flame retardants in wildlife from China: Levels, trends, and bioaccumulation characteristics, *J. Environ. Sci.*, 2012, **24**, 183–194.
  - 7 M. R. Peltier, M. J. Fassett, Y. Arita, V. Y. Chiu, J. M. Shi, H. S. Takhar, A. Mahfuz, G. S. Garcia, R. Menon and D. Getahun, Women with high plasma levels of PBDE-47 are at increased risk of preterm birth, *J. Perinat. Med.*, 2021, **49**, 439–447.
  - 8 F. Karakas, A. Aksoy and I. Imamoglu, Development of a fate and transport model for biodegradation of PBDE congeners in sediments, *Environ. Pollut.*, 2020, **266**, 115116.
  - 9 D. Zezza, S. Tait, L. D. Salda, M. Amorena, C. Merola and M. Perugini, Toxicological, gene expression and histopathological evaluations of environmentally realistic concentrations of polybrominated diphenyl ethers PBDE-47, PBDE-99 and PBDE-209 on zebrafish embryos, *Ecotoxicol. Environ. Saf.*, 2019, **183**, 109566.
  - 10 E.-J. Kim, J.-H. Kim, J.-H. Kim, V. Bokare and Y.-S. Chang, Predicting reductive debromination of polybrominated diphenyl ethers by nanoscale zerovalent iron and its implications for environmental risk assessment, *Sci. Total Environ.*, 2014, **470**, 1553–1557.
  - 11 K. S. Betts, Rapidly rising PBDE levels in North America, *Environ. Sci. Technol.*, 2002, **36**, 50A–52A.
  - 12 S. Rayne, M. G. Ikononou and M. D. Whale, Anaerobic microbial and photochemical degradation of 4,4'-dibromodiphenyl ether, *Water Res.*, 2003, **37**, 551–560.
  - 13 M. Cai, Y. Li, Y. Li and K. Du, Physiological and biochemical responses and microscopic structure changes of *Populus tomentosa* Carr seedlings to 4-BDE exposure, *Environ. Sci. Pollut. Res.*, 2015, **22**, 14258–14268.
  - 14 X. Li, J. Huang, L. Fang, G. Yu, H. Lin and L. Wang, Photodegradation of 2,2',4,4'-tetrabromodiphenyl ether in nonionic surfactant solutions, *Chemosphere*, 2008, **73**, 1594–1601.
  - 15 Y.-H. Shih, H.-L. Chou and Y.-H. Peng, Microbial degradation of 4-monobrominated diphenyl ether with anaerobic sludge, *J. Hazard. Mater.*, 2012, **213**, 341–346.
  - 16 S. Krol, B. Zabiegala and J. Namiesnik, Determination of polybrominated diphenyl ethers in house dust using standard addition method and gas chromatography with electron capture and mass spectrometric detection, *J. Chromatogr. A*, 2012, **1249**, 201–214.
  - 17 G. Martinez, J. Niu, L. Takser, J. P. Bellenger and J. Zhu, A review on the analytical procedures of halogenated flame retardants by gas chromatography coupled with single quadrupole mass spectrometry and their levels in human samples, *Environ. Pollut.*, 2021, **285**, 117476.
  - 18 H. S. Hendriks, E. C. A. Fernandes, A. Bergman, M. van den Berg and R. H. S. Westerink, PCB-47, PBDE-47, and 6-OH-PBDE-47 Differentially Modulate Human GABA(A) and  $\alpha(4)\beta(2)$  Nicotinic Acetylcholine Receptors, *Toxicol. Sci.*, 2020, **118**, 635–642.
  - 19 J. W. Hu, E. Kolehmainen and J. Knuutinen, H-1 and C-13 NMR spectroscopy of brominated diphenyl ethers. A multiple linear regression analysis, *Magn. Reson. Chem.*, 2000, **38**, 375–378.
  - 20 A.-M. Geller, H.-U. Krueger, Q. Liu, C. Zetzsch, M. Elend and A. Preiss, Quantitative H-1 NMR-analysis of technical octabrominated diphenylether DE-79 (TM) and UV spectra of its components and photolytic transformation products, *Chemosphere*, 2008, **73**, S44–S52.
  - 21 X. Jiang, Y. Lai, W. Wang, W. Jiang and J. Zhan, Surface-enhanced Raman spectroscopy detection of polybrominated diphenylethers using a portable Raman spectrometer, *Talanta*, 2013, **116**, 14–17.
  - 22 H. Shan, C. Liu, Z. Wang, T. Ma, J. Shang and D. Pan, A fluorescence-based method for rapid and direct determination of polybrominated diphenyl ethers in water, *J. Anal. Methods Chem.*, 2015, **2015**, 853085.
  - 23 F. Bettazzi, T. Martellini, W. L. Shelper, A. Cincinelli, E. Lanciotti and I. Palchetti, Development of an Electrochemical Immunoassay for the Detection of Polybrominated Diphenyl Ethers (PBDEs), *Electroanalysis*, 2016, **28**, 1817–1823.
  - 24 H. Feng, L. Zhou, L. Shi, W. Li, L. Yuan, D. Li and Q. Cai, Development of enzyme-linked immunosorbent assay for determination of polybrominated diphenyl ether BDE-121, *Anal. Biochem.*, 2014, **447**, 49–54.
  - 25 Y. Huang, T. Xu, Y. Luo, C. Liu, X. Gao, Z. Cheng, Y. Wen and X. Zhang, Ultra-Trace Protein Detection by Integrating Lateral Flow Biosensor with Ultrasound Enrichment, *Anal. Chem.*, 2021, **93**, 2996–3001.
  - 26 D. Quesada-Gonzalez, A. Baiocco, A. A. Martos, A. de la Escosura-Muniz, G. Palleschi and A. Merkoci, Iridium oxide (IV) nanoparticle-based electrocatalytic detection of PBDE, *Biosens. Bioelectron.*, 2019, **127**, 150–154.
  - 27 G. Hanrahan, D. G. Patil and J. Wang, Electrochemical sensors for environmental monitoring: design, development and applications, *J. Environ. Monit.*, 2004, **6**, 657–664.
  - 28 C. S. Pundir and N. Chauhan, Acetylcholinesterase inhibition-based biosensors for pesticide determination: a review, *Anal. Biochem.*, 2012, **429**, 19–31.
  - 29 J. S. Van Dyk and B. Pletschke, Review on the use of enzymes for the detection of organochlorine, organophosphate and carbamate pesticides in the environment, *Chemosphere*, 2021, **82**, 291–307.
  - 30 S. Rodriguez-Mozaz, M. J. L. de Alda and D. Barcelo, Biosensors as useful tools for environmental analysis and monitoring, *Anal. Bioanal. Chem.*, 2006, **386**, 1025–1041.



- 31 K. A. Law and S. P. J. Higson, Sonochemically fabricated acetylcholinesterase micro-electrode arrays within a flow injection analyser for the determination of organophosphate pesticides, *Biosens. Bioelectron.*, 2005, **20**, 1914–1924.
- 32 V. G. Andreou and Y. D. Clonis, A portable fiber-optic pesticide biosensor based on immobilized cholinesterase and sol-gel entrapped bromocresol purple for in-field use, *Biosens. Bioelectron.*, 2002, **17**, 61–69.
- 33 C. A. Huang, L. Zhou, J. Li, L. Chen, L. Yuan, L. Shi and Q. Cai, A Highly Sensitive Electrochemical Immunosensor For The Rapid Detection Of Tris(2,3-Dibromopropyl) Isocyanurate, *Anal. Lett.*, 2014, **47**, 778–794.
- 34 R. Wilson and A. P. F. Turner, Glucose-Oxidase – An Ideal Enzyme, *Biosens. Bioelectron.*, 1992, **7**, 165–185.
- 35 T. Kuila, S. Bose, P. Khanra, A. K. Mishra, N. H. Kim and J. H. Lee, Recent advances in graphene-based biosensors, *Biosens. Bioelectron.*, 2011, **26**, 4637–4648.
- 36 L. Liu, Q. Ma, Y. Li, Z. Liu and X. Su, A novel signal-off electrochemiluminescence biosensor for the determination of glucose based on double nanoparticles, *Biosens. Bioelectron.*, 2015, **63**, 519–524.
- 37 N. G. Bastus, J. Comenge and V. Puntès, Kinetically Controlled Seeded Growth Synthesis of Citrate-Stabilized Gold Nanoparticles of up to 200 nm: Size Focusing versus Ostwald Ripening, *Langmuir*, 2011, **27**(2011), 11098–11105.
- 38 H. Razmi and R. Mohammad-Rezaei, Graphene quantum dots as a new substrate for immobilization and direct electrochemistry of glucose oxidase: Application to sensitive glucose determination, *Biosens. Bioelectron.*, 2013, **41**, 498–504.
- 39 Y. R. Kim, S. Bong, Y. J. Kang, Y. Yang, R. K. Mahajan, J. S. Kim and H. Kim, Electrochemical detection of dopamine in the presence of ascorbic acid using graphene modified electrodes, *Biosens. Bioelectron.*, 2020, **25**, 2366–2369.
- 40 X. Y. Bai and K. K. Shiu, Spontaneous Deposition of Prussian Blue on Reduced Graphene Oxide - Gold Nanoparticles Composites for the Fabrication of Electrochemical Biosensors, *Electroanalysis*, 2015, **27**, 74–83.
- 41 A. Denisenko, G. Jamornmarn, H. El-Hajj and E. Kohn, pH sensor on O-terminated diamond using boron-doped channel, *Diamond Relat. Mater.*, 2007, **16**, 905–910.
- 42 H. X. Ju and C. Z. Shen, Electrocatalytic reduction and determination of dissolved oxygen at a poly(nile blue) modified electrode, *Electroanalysis*, 2001, **13**, 789–793.

